World Academy of Science, Engineering and Technology
International Journal of Mechanical and Mechatronics Engineering
Vol:9, No:4, 2015

# Development of a Three-Dimensional-Flywheel Robotic System

Chung-Chun Hsiao, Yu-Kai, Ting, Kai-Yuan Liu, Pang-Wei Yen, Jia-Ying Tu



***Abstract*—**In this paper, a new design of spherical robotic system based on the concepts of gimbal structure and gyro dynamics is presented. Robots equipped with multiple wheels and complex steering mechanics may increase the weight and degrade the energy transmission efficiency. In addition, the wheeled and legged robots are relatively vulnerable to lateral impact and lack of lateral mobility. Therefore, the proposed robotic design uses a spherical shell as the main body for ground locomotion, instead of using wheel devices. Three spherical shells are structured in a similar way to a gimbal device and rotate like a gyro system. The design and mechanism of the proposed robotic system is introduced. In addition, preliminary results of the dynamic model based on the principles of planar rigid body kinematics and Lagrangian equation are included. Simulation results and rig construction are presented to verify the concepts.

***Keywords*—** Gyro, gimbal, Lagrange equation, spherical robots.

## I. Introduction

MANY modern robotic and vehicle systems adopt wheeled structures to achieve ground locomotion. Because the robot or vehicle designs include multiple wheels requires steering and transmission mechanism to connect and transfer power energy to wheels, their lateral mobility and energy consumption efficiency may be reduced. In the robotic literature, the concepts of single wheel robot [1], [2] are proposed, which provide the advantages over multi-wheeled robots in terms of improved mobility, reduced weight, and simplified steering and power mechanisms. Reference [2] shows an example of single-wheel robot, called *gyrover*. Two dished wheels are connected as the exterior shell, and a gyroscopic device was installed inside for stabilization. The actuation systems to drive the *gyrover* include three parts: (1) a suspended flywheel is rotated by a motor with high speed to stabilize the robot; (2) a motor is installed to control the tilt angle of the flywheel; (3) the two dished wheels are driven by a motor to roll forward/backward. Accordingly, the first two motors connected to the flywheel can control the rotation axis of the flywheel that results in a gravitationally induced torque and enables the rolling robot to turn. In this way, the steering mechanism of the robot is simplified with improved lateral mobility.

Research supported by the Taiwan Ministry of Science and Technology under Grant MOST 102-2221-E-007-109-MY2.

C. C. Hsiao, C. E. Tsai, P. W. Yen, and K. Y. Liu are with the Department of Power Mechanical Engineering National Tsing Hua University, Hsinchu 300, Taiwan (e-mail: en54612002@hotmail.com, tsai_chenen@hotmail.com, bmy2054@yahoo.com.tw, k242424123@yahoo.com.tw, respectively).

J. Y. Tu is with the Department of Power Mechanical Engineering, National Tsing Hua University, Hsinchu 300, Taiwan (Tel.:+886-3-5742497; e-mail: jytu@pme.nthu.edu.tw).

On the other hand, a new wheeled structure for vehicle design is proposed by [3], called Edward diwheel. The wheels are enlarged to become the main vehicle skeleton to protect the passengers and power units inside. Smaller inner wheels are anchored to the outer wheel to drive the vehicle. Therefore, the required power transmission and steering mechanism are simplified.

The previous two examples of improved wheeled robot and vehicle show an important design feature that, the wheels are not only used for locomotion, but also function like a solid frame for safety and protection. With the similar advantage of protecting the internal devices, the design of spherical robot receives considerable attention in recent years. Spherical robot uses a spherical shell to cover and protect the internal mechanical frames, control devices, and power units. In addition, the spherical structure enables the robot to move omnidirectionally with excellent mobility. In the presence of lateral impact, the spherical robot can be stabilized and balanced without fall-over. Several design concepts are proposed for stabilizing spherical robots, such as pendulum [4]-[8], and omnidirectional wheels [7]. Take the pendulum-driven spherical robot as an example, inside the robot a motor is installed to vibrate a pendulum device, which changes the center of mass of the robot. Therefore, a gravity-induced torque exerts the spherical robot to roll.

However, the pendulum-driven spherical robots present challenge in controlling the propulsion force, because the dynamic model between the gravity-induced torque and the rolling velocity is difficult to determine [8]. Therefore, many gimbal-like spherical robotic designs are proposed, for example, the micro air vehicle shown in [9], [10]. The motors directly drive the spherical shell to roll; thus, the trajectory can be planned in a simpler manner than the pendulum-driven robots.

From the above literature discussion, it is noted that the "foot" of robot is used not only for locomotion, but also for protecting the inner devices. In addition, considering different factors related to energy consumption, mobility, and safety, a unique design of spherical robot, with reference to the gimbal structure and gyro dynamics, is proposed in this paper, named three-dimensional-flywheel (3DF) robotic system. The outline of this paper is structured as follows. In section II, the concept and design of the 3DF robot is introduced, on the basis of gimbal mechanism, gyro effects, and spherical structure. Section III derives the dynamic model for the 3DF robot relate to forward/backward motion and spinning dynamics, using the planar rigid body kinematics and the Lagrangian method. In Section IV, the 3DF robotic design is verified via simulation, and the rig construction for implementation work is introduced.

Finally, conclusion and future work is provided in Section V.

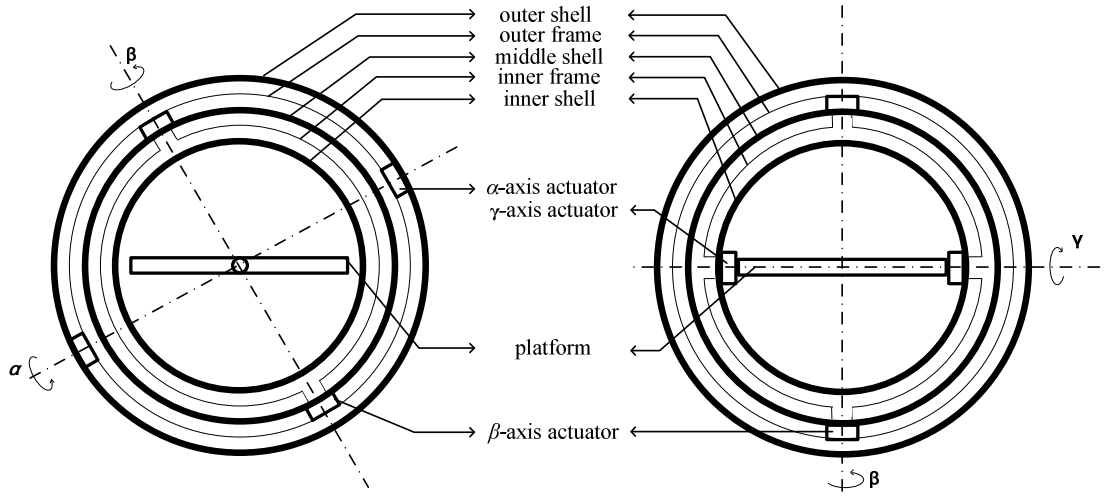


(a) Front view (b) Side view

Fig. 1 The scheme of the 3DF robot

## II. The Design Concept of the 3DF Robot

In this section, the proposed unique design of the 3DF robot is introduced; the front view and side view of the system are shown in Figs. 1 (a) and (b), respectively. The 3DF robot comprises of three spherical shells, named outer shell, middle shell, and inner shell, respectively. The rotation axes of the three shells are defined as $\alpha$ axis, $\beta$ axis, and $\gamma$ axis, respectively; the three axes are orthogonal. A platform installed within the inner shell can be used for control operation and storage, which could possibly install electronic circuits, batteries, servo controllers, sensors, balancing mechanism, etc.

To roll or rotate the three shells, a plurality of actuators are installed to the shells, called $\alpha$-axis actuator, $\beta$-axis actuator, and $\gamma$-axis actuator, which drive the outer shell, middle shell, and inner shell, respectively. In addition, the platform is connected to the inner shell via the $\gamma$-axis actuator. As the $\alpha$-axis actuator rotates the outer shell, the 3DF robot roll forward/backward. When the 3DF robot stays on a point, the rotation of the middle shell by the $\beta$-axis actuator exerts the outer shell to roll and turn, according to conservation of angular momentum. Furthermore, the $\gamma$-axis actuator in connection with the inner shell is used for balancing the 3DF robot.

Because the rotors of the actuators are connected to the three shells, and the bases of the actuators are anchored to two ring frames, the 3DF robot looks like the gimbal structure in a gyroscope, and the three shells function like three-dimensional flywheels for storing rotational energy. In the long term with better understanding of the dynamics and better control of the actuators, it is expected that the 3DF robot can provide the following unique advantages: (i) the stored rotation energy of the middle and inner shells can be used to complete a turn task, thus saving the actuation energy; (ii) the direct-driven method of the outer shell can achieve fast motion and better trajectory planning.

TABLE I
Notation and Parameters

| Notation | Parameters | ADAMS value/unit |
|---|---|---|
| $I_1$ | moment of inertia of outer shell | 96.9 kg·m$^2$ |
| $I_2$ | moment of inertia of middle shell | 72.9 kg·m$^2$ |
| $J_1$ | moment of inertia of outer frame | 2.7 kg·m$^2$ |
| $M_1$ | mass of the outer shell | 146.8 kg |
| $M_2$ | mass of the middle shell | 173.1 kg |
| $R_1$ | radius of the other shell | 1 m |
| $R_2$ | radius of the middle shell | 0.9 m |
| $m_1$ | mass of the outer frame | 5 kg |
| $x_G$ | $x$-axis displacement of center of mass | |
| $\alpha$ | α-axis rotation angle of outer spherical shell | |
| $\beta$ | $\beta$-axis rotation angle of middle spherical shell | |
| $\gamma$ | $\gamma$-axis rotation angle of inner spherical shell | |
| $\tau_\alpha$ | $\alpha$-axis motor torque | |
| $\tau_\beta$ | $\beta$-axis motor torque | |
| $\mu$ | coefficient of static friction | |

The operation and control process of the 3DF robot is shown in Fig. 2. First, the remote control center sends the trajectory reference signal to the controller within the 3DF robot. Afterward, the controller sends the control signals to the actuators to rotate the three shells for forward/backward movement and change of direction. Then, the sensors for detecting the speed of motor rotation and yaw angle feed the measured signals back to the controller to form a closed-loop control system. The controller is designed based the dynamic models and kinematics of the 3DF robot. More detailed design of the control system comprises the authors' ongoing work.

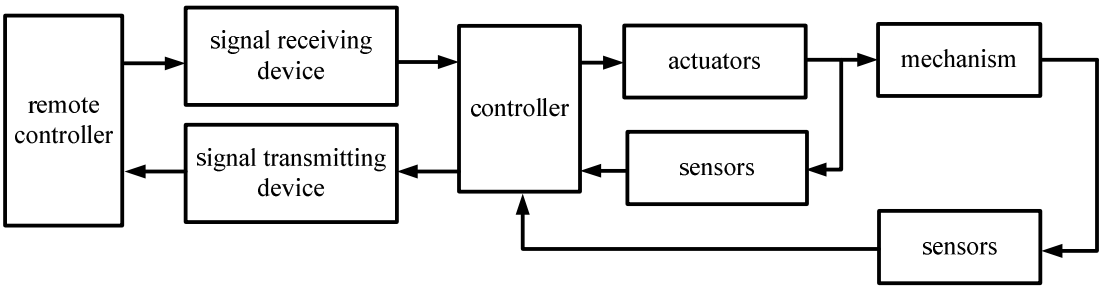


Fig. 2 The scheme of the control system

## III. Dynamic Model

This section derives the dynamic model of the 3DF robot as it rolls along a straight line in the $x$-axis direction; the coordinate system is indicated in Fig. 6. In addition, the preliminary dynamic model for spinning dynamics with respect to the $\beta$ axis is also discussed. The following assumptions are made in the mathematic model: (a) the robot rolls and spins on a horizontal plane; (b) the robot rolls without slipping; (c) the center of mass of the robot is at the geometric center itself. To simplify the discussion, only the outer shell, outer frame, and middle shell are considered in the present work.

### *A. The Equation of Motion for X-Axis Motion*

Here, the $x$-axis motion of the 3DF robot is derived on the basis of planar rigid body kinematics. Figs. 3 and 4 present the free body diagram and effective force diagram, respectively, and the outer shell is separated from the outer frame. The outer shell, outer frame, and middle shell are drawn in red, black, and blue, respectively. Only the torque generated by the $\alpha$-axis actuator is considered, that results in $x$-axis motion of the robot. The masses of the outer shell, middle shell, and outer frame are denoted as $M_1$, $M_2$, and $m_1$, respectively. In Fig. 3 the center of mass and the center of geometry of the robot are the same, denoted as $G$; the ground contact point is denoted as $O$. The relevant notation and parameters are summarized in Table I. Therefore, according to the free body diagrams in Fig. 3 and the effective force diagram in Fig. 4, the applied $x$-axis forces are given by

$$\text{outer shell:} \quad \mu N - F_x = M_1 \ddot{x}_G, \tag{1}$$

$$\text{outer frame + middle shell:} \quad F_x = (m_1 + M_2)\ddot{x}_G. \tag{2}$$

where $F_x$ denotes the $x$-axis reaction force due to the $\alpha$-axis actuator, $\mu$ is the coefficient of static friction, $\ddot{x}_G$ denotes the $x$-axis acceleration of the center of mass, and the normal force applied to $O$ is written as $N$. Similarly, the equilibrium equations for the $z$-axis forces in Fig. 3 are given by

$$\text{outer shell:} \quad N - M_1 g = F_z, \tag{3}$$

$$\text{outer frame + middle shell:} \quad F_z = (m_1 + M_2)g. \tag{4}$$

Therefore, from (1)-(4) the normal force $N$ and the $x$-direction friction force at the contact point $O$ are written as

$$N = (M_1 + m_1 + M_2)g \tag{5}$$

and

$$\mu N = (M_1 + m_1 + M_2)\ddot{x}_G, \tag{6}$$

respectively.

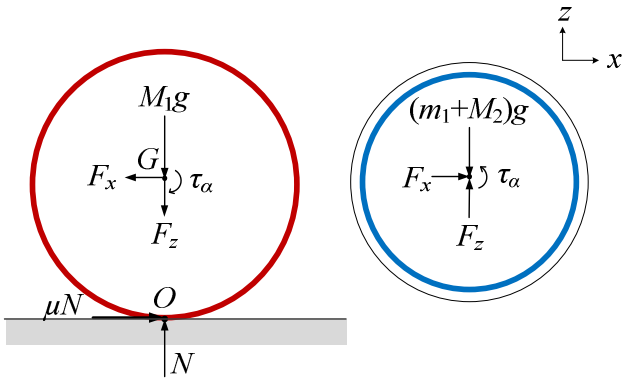


Fig. 3 Free body diagram for the $x$-axis motion

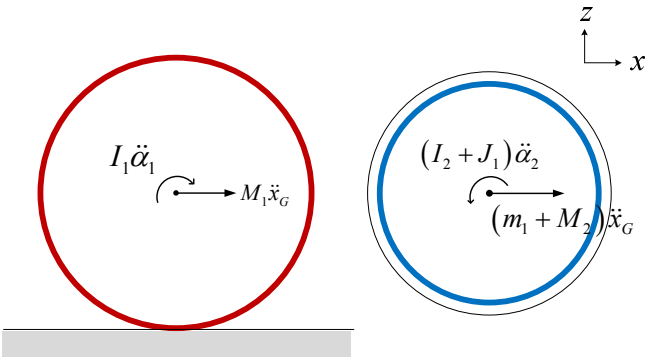


Fig. 4 Effective force diagram for the $x$-axis motion

Furthermore, Fig. 3 is transformed into the effective force diagram in Fig. 4. The $\alpha$-axis actuator drives the robot to roll forward, thus $\ddot{\alpha}_1$ denotes the $\alpha$-axis angular acceleration of the outer shell, $\ddot{\alpha}_2$ denotes the $\alpha$-axis angular acceleration of the outer frame and middle shell due to the reaction torque. The total moment acting on $G$ is equal to the rate of change of angular momentum as

$$\text{outer shell:} \quad \tau_\alpha - \mu N R_1 = I_1 \ddot{\alpha}_1, \tag{7}$$

outer frame + middle shell: $\tau_\alpha = (J_1 + I_2)\ddot{\alpha}_2$. (8)

Here $\tau_\alpha$, is the $\alpha$-axis motor torque, $R_1$ is the radius of outer shell, and the moment of inertia, $I_1$, is given by

$$I_1 = \frac{2}{3} M_1 R_1^2. \quad (9)$$

In addition, according to the assumption that the robot rolls without slipping, the ideal relationship between $\ddot{x}_G$ and $\ddot{\alpha}_1$ is shown as

$$\ddot{x}_G = R_1 \ddot{\alpha}_1. \quad (10)$$

With the substitution of (6), (9) and (10) into (7) and (8) yields

$$\tau_\alpha = \left[ I_1 + R_1^2 (M_1 + m_1 + M_2) \right] \ddot{\alpha}_1 = (J_1 + I_2) \ddot{\alpha}_2. \quad (11)$$

Equation (11) shows the equation of motion of the 3DF robot with $x$-axis motion, and the relationship between $\ddot{\alpha}_1$ and $\ddot{\alpha}_2$ is obtained.

*B. The Equation of Motion for B-Axis Spin*

In this section, the spinning motion of the 3DF robot is discussed, which means that the $\beta$-axis actuator rotates the middle shell results in a reaction torque to the outer shell. Thus, the outer shell/the robot spins along the $\beta$ axis. To derive the equation of motion for the spinning dynamics of the 3DF robot, the Lagrangian method is used. The typical form of Lagrange equation is given by

$$\frac{d}{dt}\left( \frac{\partial L}{\partial \dot{q}_i} \right) - \frac{\partial L}{\partial q_i} = Q_i, \; i = 1, 2, ..., n, \quad (12)$$

where $L$ is the Lagrangian, $Q_i$ represents generalized force, $q_i$ is generalized coordinate, and $n$ is the number of independent coordinates. The Lagrangian $L$ is expressed as $L = T - V$, where $T$ and $V$ are the kinetic and potential energy, respectively.

As shown in the top view of Fig. 5 related to the $\beta$-axis spinning dynamics, the $\beta$-axis actuator drives the middle shell to generate the rotation angle $\beta_2$. Meanwhile, the rotation of the outer frame and outer shell are synchronized; their rotation angle is denoted as $\beta_1$. Thus, the rotational kinetic energy of the 3DF robot with respect to the shells and frame is obtained as follows

$$T = \frac{1}{2}(I_1 + J_1)\dot{\beta}_1^2 + \frac{1}{2} I_2 (\dot{\beta}_1 - \dot{\beta}_2)^2, \quad (13)$$

where $I_2$ and $J_1$ are the moment of inertia of the middle shell and the outer frame, respectively, and $\dot{\beta}_1 - \dot{\beta}_2$ denotes the absolute angular velocity of the middle shell with respect to ground.

Furthermore, when the shells rotate along the $\pm\beta$ axes, the potential energy does not change because the center of mass of the robot is unchanged, given by

$$V = (M_1 + m_1 + M_2) g R_1. \quad (14)$$

Subtract (14) from (13) gives the Lagrangian as follows

$$L = \frac{1}{2}(I_1 + J_1)\dot{\beta}_1^2 + \frac{1}{2} I_2 (\dot{\beta}_1 - \dot{\beta}_2)^2 - (M_1 + m_1 + M_2) g R_1. \quad (15)$$

In addition, the generalized coordinate is defined as $q_1 = \beta_1$, and the generalized force are determined as $Q_1 = \tau_f$, where $\tau_f$ is a friction torque acting on the contact point $O$. Therefore, with the substitution of (15) into (12) and considering the generalized force, the Lagrange equation is given by

$$\frac{d}{dt}\left( \frac{\partial L}{\partial \dot{\beta}_1} \right) - \frac{\partial L}{\partial \beta_1} = \tau_f. \quad (16)$$

Expand (16) yields the following equation of motion

$$\ddot{\beta}_1 = \frac{1}{(I_1 + J_1 + I_2)} \tau_f + \frac{I_2}{(I_1 + J_1 + I_2)} \ddot{\beta}_2. \quad (17)$$

Thus, the relationship between angular acceleration $\ddot{\beta}_1$ and $\ddot{\beta}_2$ is obtained. Then, according to the moment of momentum theorem with respect to the $z$ axis, the relationship between $\tau_\beta$, $\tau_f$, and $\ddot{\beta}_2$ is given as

$$\tau_f + \tau_\beta = (I_1 + J_1 + I_2)\ddot{\beta}_2. \quad (18)$$

Equations (5)-(18) preliminarily derive the equations of motion related to the $\alpha$- and $\beta$-axis dynamics. However, in this section the rotation of the inner shell and the coupled dynamics between each axis are not considered yet. Future work on the derivation of complete dynamic model will be carried out.

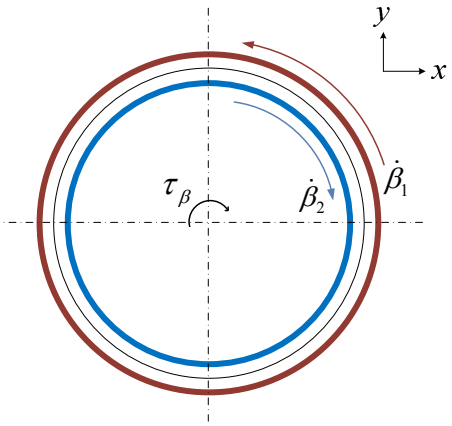


Fig. 5 Top view of the $\beta$-axis spinning dynamics

## IV. Simulation Studies and Implementation Work

This section uses the commercial software ADAMS to simulate the design and motion of the 3DF robot. The relevant parameters are summarized in Table I. The model in ADAMS contains an outer shell, an outer frame, a middle shell, and $\alpha$-axis and $\beta$-axis actuators, as shown in Fig. 6. The rotation

axes of the $\alpha$-axis and $\beta$-axis actuators are orthogonal.

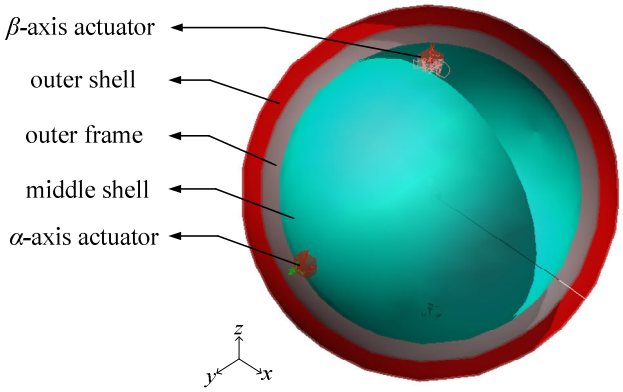


Fig. 6 The ADAMS model of the 3DF robot

In the simulation work of Fig. 7, the $\alpha$-axis actuator is driven with a constant angular velocity to roll the outer shell forward, and the $\beta$-axis actuator is driven with a non-constant torque, as shown in Fig. 7 (a). Therefore, in the first 5 seconds of the simulation, only the $\alpha$-axis actuator inputs torque to roll the outer shell. Later on, the time-varying $\beta$-axis actuator torque is added to rotate the middle shell in the $5^{th}$ to $10^{th}$ seconds. Fig. 7 (b) shows the trajectory of $G$ from the top view on the $x$-$y$ plane. The robot rolls smoothly along a straight line in the $x$ axis for about 10 m, because only the $\alpha$-axis actuator drives the outer shell to roll. Then the robot's trajectory becomes like a curve because the $\beta$-axis actuator rotates the middle shell to make the robot turn right. Therefore, Fig. 7 (b) verifies that the 3DF robot design is able to achieve straight line motion and turn, via the rotations of the outer and middle shells.

Furthermore, the velocity signals of the point $G$ are shown in Figs. 7 (c) and (d), where $\dot{x}_G$ and $\dot{y}_G$ denote the $x$-axis and $y$-axis velocities, respectively. In the first five seconds, the $\dot{x}_G$ signal increases and then reduces to negative values. The $\dot{y}_G$ signal is zero in the first five seconds because the middle shell does not rotate and affect the $y$-axis motion. After the fifth second, the $\dot{y}_G$ signal changes in a similar pattern to that of Fig. 7 (a).

However, the responses in Figs. 7 (b) and (d) show undesired oscillation starting from the thirteenth second. The possible reason for the undesired responses is that the outer frame rotation due to the reaction torque incurs vibration. For example, because of the reaction force produced by the α-axis actuator, the outer frame and middle shell would rotate in opposite direction. Thus, the output velocities become oscillating. In order to solve this problem, it is necessary to design an additional mechanism to fix the outer frame and to stabilize the system.

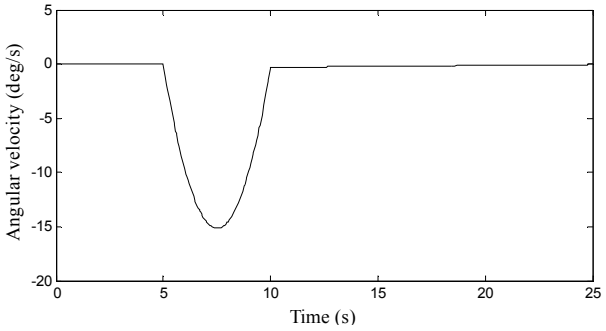


(a) The $\beta$-axis actuator input signal

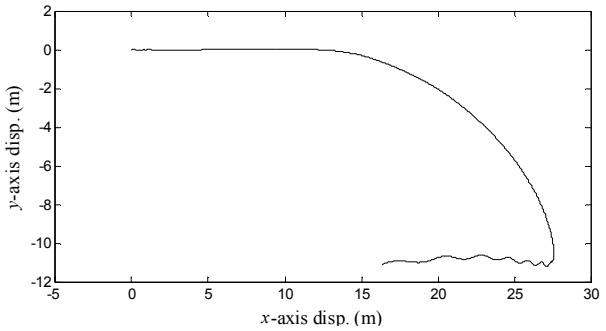


(b) The trajectory of point $G$ in the $x$-$y$ plane

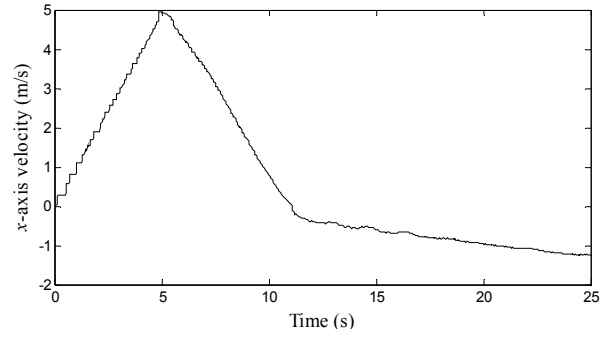


(c) The $\dot{x}_G$ signal

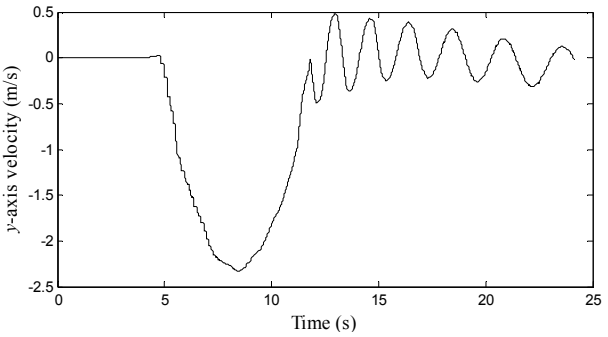


(d) The $\dot{y}_G$ signal

Fig. 7 ADAMS simulation results

On the other hand, with the design concept introduced in Section II, a preliminary prototype of the 3DF robot is shown in Fig. 8. The rig includes outer shell, a platform, and two spinning disks for control purpose. The outer shell is driven by

two motors, which are defined as the $\alpha$-axis actuator. A motor is connected to a spinning disk underneath the platform. As the disk rotates, the robot is able to turn based on the principle of conservation of angular momentum. However in practice, as the $\alpha$-axis actuator rolls the robot moves forward, the platform rocks back and forth due to the reaction torque from $\tau_\alpha$. Therefore, as the outer shell rolls, the second disk on the platform also spins in order to balance the platform. In our future implementation work, control system design for the prototype in Fig. 2 will be carried on, and the mechanical design of the middle shell for steering will be considered.

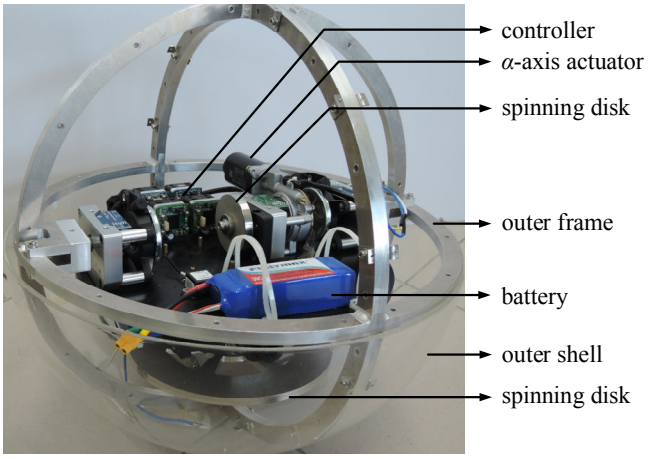


Fig. 8 The preliminary prototype of the 3DF robot

## V. Conclusion

A new three-dimensional-flywheel (3DF) robotic system is proposed in this paper, based on the concepts of gimbal mechanism and gyro dynamics. The system contains three shells which act like three-dimensional flywheels to store rotational energy. The principle of mechanical design, mechanism, and control system are introduced. In addition, the equations of motion of the system are preliminarily derived using the techniques of planar rigid body kinematics, Lagrangian equation, and conservation of angular momentum. Finally, the simulation results using the ADAMS models are presented, and a prototype of the robot is introduced. The simulation and implementation work show that, with the spherical structure, the 3DF robot would be considered an enlarged gyroscope, which is able to achieve self-balance and fast steering. Future work on the derivation of the dynamic model, mechanical design, and control system design of the complete 3DF robot will be carried on.

## Acknowledgment

The authors gratefully acknowledge the support of Taiwan Ministry of Science and Technology, under grant 102-2221-E-007-109-MY2 '*Evaluation of Optimal Dynamic Substructuring Tests*: *Development and Application of Substructurability Theory*', for their support in the pursuance of this work. Also, the authors are grateful to the National Center for High-performance Computing for computer time and facilities.

## References

[1] H. B. Brown, Jr. and X. Yangsheng, "A single-wheel, gyroscopically stabilized robot," New York, NY, USA, 1996, pp. 3658-63.
[2] X. Yangsheng, H. B. Brown, Jr., and A. Kwok Wai, "Dynamic mobility with single-wheel configuration," vol. 18, pp. 728-38, 07/ 1999.
[3] B. Cazzolato, J. Harvey, C. Dyer, K. Fulton, E. Schumann, T. Zhu*, et al.*, "Modeling, simulation and control of an electric diwheel," in *Australasian Conference on Robotics and Automation*, Melbourne, VIC, Australia, 2011, p. Australian Robotics and Automation Association Inc.; Monash University.
[4] R. Chase and A. Pandya, "A Review of Active Mechanical Driving Principles of Spherical Robots," vol. 1, pp. 3-23, / 2012.
[5] A. Halme, T. Schonberg, and W. Yan, "Motion control of a spherical mobile robot," in *Proceedings of 4th IEEE International Workshop on Advanced Motion Control* New York, NY, USA, 1996, pp. 259-64.
[6] K. Jayoung, H. Kwon, and L. Jihong, "A rolling robot: design and implementation," in *7th Asian Control Conference*, Piscataway, NJ, USA, 2009, pp. 1474-9.
[7] C. Wei-Hsi, C. Ching-Pei, Y. Wei-Shun, L. Chang-Hao, and L. Pei-Chun, "Design and implementation of an omnidirectional spherical robot Omnicron," in *IEEE/ASME International Conference on Advanced Intelligent Mechatronics*, Piscataway, NJ, USA, 2012, pp. 719-24.
[8] W.-H. Chen, C.-P. Chen, J.-S. Tsai, J. Yang, and P.-C. Lin, "Design and implementation of a ball-driven omnidirectional spherical robot," *Mechanism and Machine Theory,* vol. 68, pp. 35-48, 2013.
[9] C. E. Thorne and M. Yim, "Towards the Development of Gyroscopically Controlled Micro Air Vehicles," in *IEEE International Conference on Robotics and Automation, 9-13 May 2011*, Piscataway, NJ, USA, 2011, pp. 26-31.
[10] C. E. Thorne, "Design and analysis of a gyroscopically controlled micro air vehicle," 3498010 Ph.D., University of Pennsylvania, Ann Arbor, 2011.